Materials and Design 115 (2017) 82–92

Contents lists available at ScienceDirect

Materials and Design

journal homepage: www.elsevier.com/locate/matdes

Effectiveness of oxalic acid treatments for the protection of marble surfaces

A. Burgos-Cara *, E. Ruiz-Agudo, C. Rodriguez-Navarro

Department of Mineralogy and Petrology, University of Granada, 18071 Granada, Spain

HIGHLIGHTS

- Marble treatment with low pH oxalic acid results in protective pseudomorphic oxalate rims.
- The oxalic acid treatment is effective against chemical weathering.
- No significant color changes were observed on treated calcitic and dolomitic marbles after treatment.

GRAPHICAL ABSTRACT

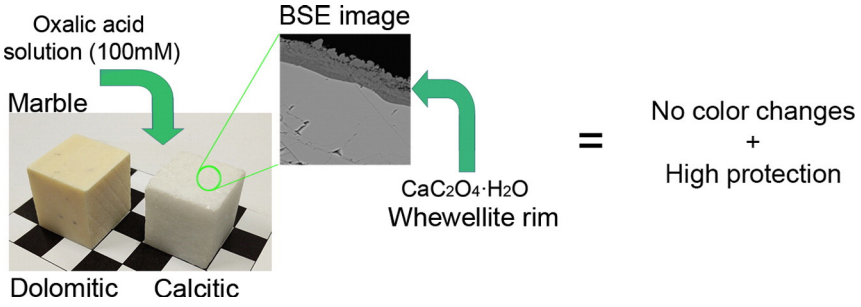

ARTICLE INFO

Article history:
Received 4 July 2016
Received in revised form 4 November 2016
Accepted 9 November 2016
Available online 12 November 2016

Keywords:
Oxalate
Marble
Whewellite
Glushinskite
Protective treatment

ABSTRACT

Naturally formed rims of calcium oxalates developed on calcareous stones have been recognized as effective protective coatings. Inspired in nature, it has been recently proposed the use of oxalate salts for the protection of stone surfaces via dissolution of the calcitic substrate and the subsequent precipitation of oxalate phases. In contrast, the application of an oxalic acid solution on carbonate stones has been generally avoided due to assumed hazards associated with enhanced substrate dissolution. Nonetheless, it has been reported that coherent oxalate layers and preservation of textural features only occurs at low pH, which could be beneficial from a conservation point of view. Here, the application of oxalic acid treatments on two calcitic and dolomitic Spanish marbles from Macael area has been studied as a means to develop effective oxalate protective coatings. Morphological and compositional analyses show that reacted marble surfaces develop μm-thick calcium or calcium and magnesium oxalate rims on calcitic and dolomitic marble, respectively. The presence of such oxalate layers strongly reduces chemical weathering due to acid dissolution and sulfation, without altering the color of the marble substrates. This protection methodology overcomes the limitations of previous oxalate treatments and may represent a highly efficient conservation methodology.

1. Introduction

Calcium oxalate films developed on stone substrates, have been found on several ancient monuments such as the Parthenon [1], the Coliseum [2], the Trajan's column [3] and even on the Moai Statues in Easter Island [4]. Despite extensive research, a thorough understanding of the causes leading to their formation has not been achieved. This has resulted in a considerable controversy, with several hypothesis put forward to explain their origins [5,6].

One school of thought considers that protective oxalate films or rims found on stone are anthropogenic, and they result from several attempts made in the past to protect and conserve stone cultural heritage [7,8]. It is known that different plants, fruits and their juices, as wells as

* Corresponding author.
E-mail address: aburgoscara@ugr.es (A. Burgos-Cara).

http://dx.doi.org/10.1016/j.matdes.2016.11.037
0264-1275/

other common organic products (e.g., casein, milk or egg yolk) were used by ancient cultures for surface finishing and/or protection of stone used in statuary and buildings [9]. Davidovits et al. [10]. found that the mix of blackberry bush, patience dock and sorrel has a considerable concentration of oxalic salts that in the presence of citric acid (also from plants such as *Agave americana*, among others) prompted the formation of oxalic acid. Subsequently, the reaction of this acid with the stone substrate would eventually result in the formation of sparingly soluble (Ca and/or Mg) oxalate salts, particularly on relatively acid soluble stones such as marble or limestone. The extremely low solubility of such earth-alkaline oxalates would protect the treated carbonate stone surface from further chemical weathering (i.e., dissolution and sulfation) [11]. A second path for the formation of oxalates is non-anthropogenic [6,12]. In this latter case the formation of oxalate films is induced by some microorganism. Once this path was considered, lichens were the most likely candidates because their metabolic activity results in the excretion of oxalic acid [6,13–15], leading to the formation of calcium oxalates on calcareous substrates [3,12]. Their ubiquitous presence everywhere around the world would thus help to explain why oxalate films are so common on the surface of rock outcrops [16]. The chemical action of lichens on rock substrates in nature has been widely studied and the role of oxalic acid as a lichen-related weathering agent is well documented [12,13,17–19]. Nowadays, however, the increased pollution levels in urban centers, have decreased lichens activity [6]. However, evidence of recent oxalate film formation on stone buildings located in urban centers exists [20]. Some films are produced by blue-green algae, green algae, various fungi and numerous bacteria that excrete oxalic acid as a result of their metabolism [17]. It should be considered that a combination of anthropogenic and natural paths is also possible. Indeed, it has been found that some of the ancient rudimentary treatments that mankind used for many different purposes (e.g. polishing) not necessarily contained oxalic acid or derived salts, but nutrients that enhanced the proliferation of fungi and bacteria capable of producing oxalic acid derivatives. Finally, is has been also suggested that oxalate films could form via deposition of pollution-derived oxalic acid, although such hypothesis requires further study [21].

Regardless the origin of ancient oxalate films, oxalate treatments are currently applied for stone protection, especially on marble [22–24] and limestone [24–26]. Most of them are based on the use of ammonium oxalate or diethyl oxalate, among other oxalate salts [22,24,26–29]. This means that these treatments are carried out at a relatively high pH, and result in the dissolution of calcite and the subsequent precipitation of calcium oxalate in an uncoupled process that result in a non-pseudomorphic replacement with a weak epitaxial relationship between the precipitated calcium oxalate and the calcitic substrate [30]. These conditions also lead to bigger and non-oriented crystals that increase the surface porosity [29,30]. Therefore, the developed layer has a weak cohesion being easily detachable and, as a consequence, the long term protection in not warranted. Ruiz-Agudo et al. [30]. found that the replacement of calcite single crystals by calcium oxalate monohydrate, the mineral known as whewellite, is a coupled dissolution–precipitation process where a pseudomorph can be obtained just under conditions of low pH, when calcite dissolution is controlled by mass transfer. Additionally, King et al. [23] found for Carrara marble that the higher the oxalic acid concentration and the temperature, the thicker the developed rim was. The authors observed two individual oxalate layers when using concentrations above 10 mM oxalic acid where the inner layer was often composed by smaller crystals (specially at lower temperatures) showing a more compact and durable replacement layer for marble protection. Accordingly, the use of low pH solutions was proposed due to the optimal epitaxial relationships between the calcium oxalate and the calcitic substrate resulting from a coupled dissolution-precipitation process [30]. At first, it might seem inappropriate to generate a continuous surface layer because of the negative effects often associated with the formation of impervious hard-crusts on treated stone surfaces that, for instance, result in a reduction of the water vapor permeability, among other detrimental effects. However, a protective conversion layer of up to a few tenths of μm, homogeneously covering the stone substrate and preserving its overall fluid transport properties, without negatively affecting the stone pore system, might in principle be an effective conservation treatment [24]. Nonetheless, testing of the efficacy of such a low pH oxalate conversion process for the protection of marble was not performed.

Consequently, we have investigated the use of an oxalic acid solution (low pH) for the protection of two different kinds of marble substrates. After the treatment, which was applied at room and at medium-high temperatures, we studied both the morphology and composition of the developed rims. Also, the resistance against weathering agents, possible treatment-induced surface color changes, and hydric properties were determined in order to quantify the efficacy and durability of the treatment.

2. Methodology

2.1. Materials

Non-polished test cubes (2 × 2 × 2 cm in size) of white calcitic and yellow dolomitic marble (Fig. 1) were prepared from raw quarry blocks. The two marble stones were from Macael (Almería, Spain), a quarry area that supplied most of the marble stone present in southern Spain architectural and sculptural heritage (e.g. the Alhambra).

2.2. Treatment procedure

Before treatment, every cube was washed with ultrapure type I+ water (resistivity > 18.2 MΩ·cm) and oven-dried at 60 °C until constant weight. For the protective treatment, every cube was immersed for 7 days in a 250 mL plastic container filled with 100 mL of 100 mM oxalic acid solution (pH ~ 1.7), prepared by using oxalic acid 2-hydrate (>99.5%, Panreac). The closed containers were stored either at room *T* (20 °C) or at 60 °C in order to investigate the influence of *T* on calcium oxalate rim development. After seven days, cubes were collected, rinsed in water, dried and weighted again to determine mass changes.

2.3. Analytical protocol

2.3.1. Optical microscopy

A polarized light microscope Jenapol U (Zeiss) working in transmission mode was used to analyze the textural features of thin-sections

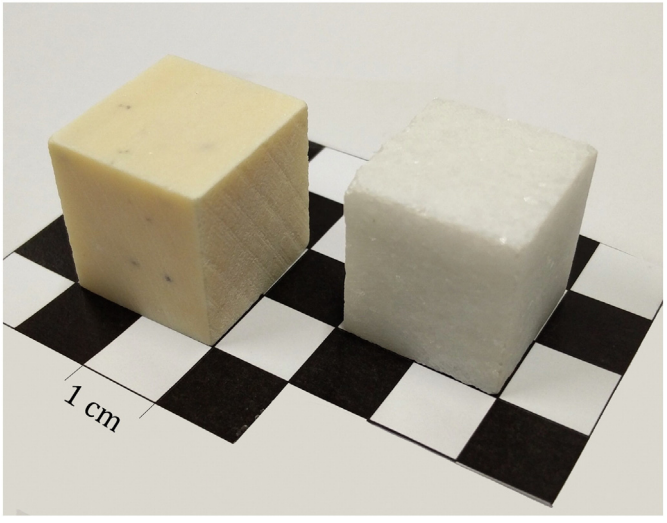

Fig. 1. Examples of marble cubes used as test samples. Left: dolomitic marble; right: calcitic white marble.

prepared from the different marbles and treatment temperatures. Thin sections were cut normal to the treated surfaces.

2.3.2. Electron microscopy

An Auriga (Carl Zeiss SMT) Field Emission Scanning Electron Microscope (FESEM) was used for morphology and texture examinations and microanalysis with energy dispersive X-ray spectroscopy (EDS). To examine the surface morphology of the samples, solids were carbon coated and secondary electron (SE) images were acquired by FESEM using the SE-inLens detector. For textural investigations, treated cubes were embedded into epoxy resin and thin sections cut normal to the sample faces were prepared. Thin sections were then carbon coated and examined by FESEM in backscattered electron mode (BSE) and element distribution maps were obtained using EDS. Observations were carried out at an accelerating voltage of 3 kV (SE) and 20 kV (BSE). Contrast in BSE mode is given by the average molecular weight of the different phases present which together with the differences in texture and EDS maps, allows discriminating between the original carbonate substrate and the developed oxalate rim.

2.3.3. Micro-RAMAN spectroscopy

Raman analyses were performed by using a Horiba Scientific LabRam HR8000 confocal Raman spectrometer. Measurements were carried out using a 100× objective with 0.9 numerical aperture, which result in a theoretical lateral resolution of 720 nm. Samples were excited with a solid state Nd:YAG laser ($\lambda = 532.09$ nm) with ~50 mW power at the sample surface. The scattered Raman light was collected in 180° backscattering geometry by an electron-multiplier charge-coupled device (CCD) detector after having pass through a 20 μm receiving slit and being dispersed by a grating of 1800 grooves/mm. Raman spectra were recorded in the 400–1200 cm^{-1} range. To increase the signal to noise ratio, the acquisition time was fixed at 30s with 3 accumulations.

2.3.4. X-ray diffraction analysis

To identify the mineralogy of the surface, an external 3 mm thick layer collected from each treated marble cube was placed in a Pananalytical X'Pert PRO diffractometer and its diffraction pattern was collected. No grinding/powdering was performed in order to preserve the original orientation and textural features of the converted layer and the substrate. The following working conditions were used: radiation CuKα ($\lambda = 1.5405$ Å), voltage 45 kV, current 40 mA, scanning angle (2θ) 3–60° and goniometer speed 0.1 °2θ s^{-1}.

2.3.5. Mercury intrusion porosimetry (MIP)

The modifications in the distribution of the pore access size as well the pore/fissure volume of marbles was determined using a Micromeritics Autopore III 9410 porosimeter with a maximum injection pressure of 414 MPa. Two replicates per treatment temperature (as well as untreated samples) of each type of marble were done. Samples with mass ca. 3 g were used. They correspond to thin slices (~2 mm in thickness) cut from the external surfaces of the sample cubes.

2.3.6. Hydric tests

The kinetics of water absorption was determined according to European Norm (EN) 13755:2010 [31]. Six cubes per treatment temperature (as well as six untreated samples) of each type of marble (as suggested by the EN) were dried at 70 °C for 24 h, weighed and immersed in type I+ water. At predetermined time increments, cubes were taken out of the water, quickly cleaned with a wet cloth for removal of excess surface water, weighed and immersed in water again. This procedure was repeated until a constant weight was reached (i.e., saturation at atmospheric pressure). Water content as percentage was calculated according to Eq. (1),

$$W(\%) = \frac{m_t - m_0}{m_0} \cdot 100 \quad (1)$$

where W(%) is the water content, m_t the sample weight for every weighing time and m_0 the initial weight of the sample.

Once a constant weight was reached, the forced water absorption capacity was determined by establishing a 10^{-3} Torr vacuum for 12 h in the recipient that contained the samples immersed in water. After that, samples were collected, quickly cleaned with a wet cloth, and weighted again.

Finally, in order to determine desorption (i.e., drying) kinetics of water-saturated samples, they were left to dry at laboratory conditions (25 °C and 30% relative humidity, RH), weighing them at predetermined time intervals until a constant weight was reached.

2.3.7. Water vapor permeability

The permeability to water vapor (WVP) was determined according to European Norm (EN) 15803:2010 [32] using the *wet cuvette* method and test samples 45 × 45 × 10 mm in size. The test device proposed by the EN (Fig. S1) was used. First, test samples were placed in a climatic chamber model KMF 5.2 (BINDER GmbH, Germany) at 23 °C and 50% RH up to constant weight. Afterwards, a saturated KNO_3 solution was placed inside the cuvette to maintain a constant 93% RH as EN suggests for *wet cuvettes* and five samples per treatment temperature (as well as five untreated samples) of each type of marble were placed again in the climatic chamber at 23 °C and 50% RH.

2.3.8. Acid-resistance batch experiments

Tests were performed by using a Titrando 905 system (Metrohm) controlled by a computer with the software Tiamo v2.5 for continuous pH recording. The system was coupled to a pH-meter (Electrode Plus mod. 6.0262.100, Metrohm), a thermostatic bath (TC-602, Brookfield) and a stirrer module (801 Stirrer, Metrohm) (Fig. S2). In order to obtain quantitative information on the acid resistance capacity of marble samples before and after treatment, the probes were fully immersed in 150 mL hydrochloric acid solution with an initial pH of 4, at 25 °C and under stirring conditions. Then, the pH was measured over time in order to determine the neutralization rate of the solution as a result of the blocks (carbonate minerals) dissolution. Three replicates per treatment temperature (as well as for untreated samples) of each type of marble were done.

2.3.9. Color changes

Color changes were determined according to CIEDE2000 [33] using a spectrophotometer Minolta CM-700 d, with the standard illuminant D65 and observer at 10°. Color coordinates L^* (luminosity or lightness which varies from black with a value of 0 to white with a value of 100), a^* (which varies from positives values for red to negatives values for green) and b^* (which varies from positives values for yellow to negatives values for blue) were measured. For each temperature, all samples were measured before and after treatment and at least 18 measurements were performed on each block: 3 on each face of the 20 mm-side cubes and 9 on the two 45 × 45 mm faces of the WVP test samples. The color change ΔE_{00} was calculated using the equations proposed by Sharma et al. [33]. and the chroma component (C^*) according to Eq. (2).

$$C^* = \sqrt{a^{*2} + b^{*2}} \quad (2)$$

2.3.10. Determination of resistance to ageing by SO_2 attack in the presence of humidity

To study the durability of the treatment and its protective effect against sulfation, the EN 13919:2003 [34] was followed to age non-treated and treated samples. Samples were immersed in water for 24 h and collected afterwards. Subsequently, they were placed in a closed acid-resistant container having a H_2SO_3 solution on its bottom with ~1.35%$_w$ SO_2 in order to generate a SO_2 saturated atmosphere

inside the container. Samples were placed 110 mm higher than the level of the acidic solution and maintained inside the container for 21 days. Afterwards, samples were weighted to determine potential mass changes and, subsequently, changes in color and surface texture were analyzed by spectrophotometry and scanning electron microscopy, respectively. Five replicates per treatment temperature (as well as for untreated samples) of each type of marble were done.

3. Results and discussion.

After seven days of immersion in the treatment solution, test cubes were collected, washed and dried until constant weight. Then, further tests and analyses were performed on randomly selected sample cubes as described in methodology. Samples are named according to Table 1.

3.1. Textural analysis

Optical microscopy observations showed continuous rims along the external surface of all marble cubes (Fig. 2). The average thickness of the rims ranged from 10 μm up to 30 μm for marble samples treated at 20 and 60 °C, respectively.

In order to characterize the rims at a higher magnification, thin-sections were carbon coated and observed in BSE mode using a FESEM (Fig. 3). FESEM analysis showed a pseudomorphic rim along the surface that even penetrated a few micrometers within the intergranular space of carbonate mineral grains making up the marble. FESEM images confirmed that both calcitic and dolomitic marble cubes treated at 20 °C developed a thinner rim (~10 μm thick) than marble cubes treated at 60 °C (~30 μm thick). In agreement with the observation reported by King et al. [23], a greater porosity is appreciable on samples treated at 60 °C due to a misorientation of the precipitated whewellite crystals on the external part of the reaction rim. On the other hand, BSE images show that the outer part of the rims reproduces the initial topography of the marble substrates, and displayed a perfect, coherent contact with the marble substrate. The oxalate rims showed a lower amount of cracks and/or porosity than those reported by Doherty et al. [11] or Mudronja et al. [26] formed on calcitic marble following treatment with ammonium oxalate.

In some areas of D60 samples, an additional external rim with a different composition appeared (Fig. 4). EDS results (Fig. 4) showed that the external rim was composed by a magnesium-bearing phase, while the inner rim was made up of a calcium-bearing phase, with different contrast in BSE mode than the underlying dolomite and calcite crystals.

In the case of the calcitic marble, just whewellite ($CaC_2O_4 \cdot H_2O$) (see Raman and XRD results, below) could precipitate due to the absence of Mg^{2+}, whereas for the dolomitic marble the precipitation of whewellite and magnesium oxalate phases, such as glushinskite ($MgC_2O_4 \cdot 2H_2O$), was thermodynamically possible under the experimental conditions for D60 samples. The distribution of precipitates shown in Fig. 4 suggests that during the interaction of the marbles with oxalic acid solutions, whewellite precipitated earlier than glushinskite due to its lower solubility (log Ksp −8.69 [35] vs log Ksp −5.18 [36], respectively). The perfect pseudomorphism observed in these partially replaced samples, resulting in the preservation of the textural features of the calcitic and dolomitic substrates, suggests that the replacement took place via an interface-coupled dissolution-precipitation mechanism [37] as previously indicated by Ruiz-Agudo et al. [30]. According to this mechanism, the dissolution of carbonate minerals present in marble generates an effective supersaturation with respect to earth-alkaline oxalate phases at the mineral-solution interface until whewellite precipitates limiting the subsequent transport of ions through this product layer. In the case of the dolomitic marble, during this initial stage, the Ca concentration decreases at the mineral-solution interface, while the Mg

Table 1
Samples identification.

C	Untreated Calcitic marble
C20	Calcitic marble treated at 20 °C
C60	Calcitic marble treated at 60 °C
D	Untreated dolomitic marble
D20	Dolomitic marble treated at 20 °C
D60	Dolomitic marble treated at 60 °C
…A	Aged samples

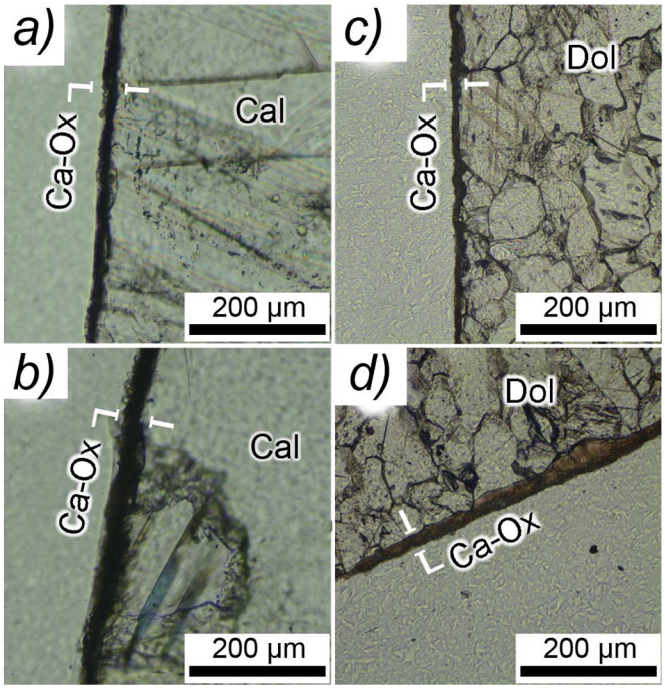

Fig. 2. Plane light optical microscopy images of thin-sections from treated cubes. Calcitic marble treated at 20 °C (a) and 60 °C (b) and dolomitic marble treated at 20 °C (c) and 60 °C (d). Legend: Cal: Calcite, Dol: Dolomite, Ca-Ox: Calcium oxalate.

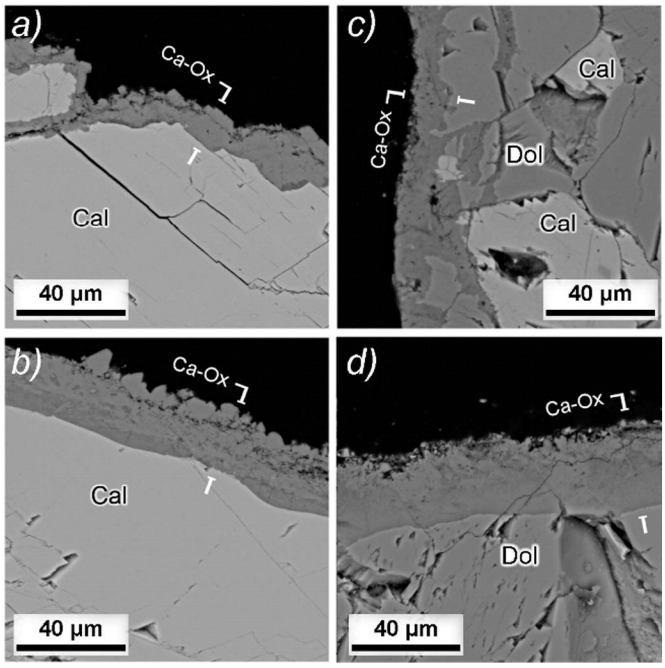

Fig. 3. BSE photomicrographs of thin-sections corresponding to a) C20, b) C60, c) D20, d) D60. The darker the color, the lower the average molecular weight of the different mineral phases. Legend: Cal: Calcite, Dol: Dolomite, Ca-Ox: Calcium oxalate.

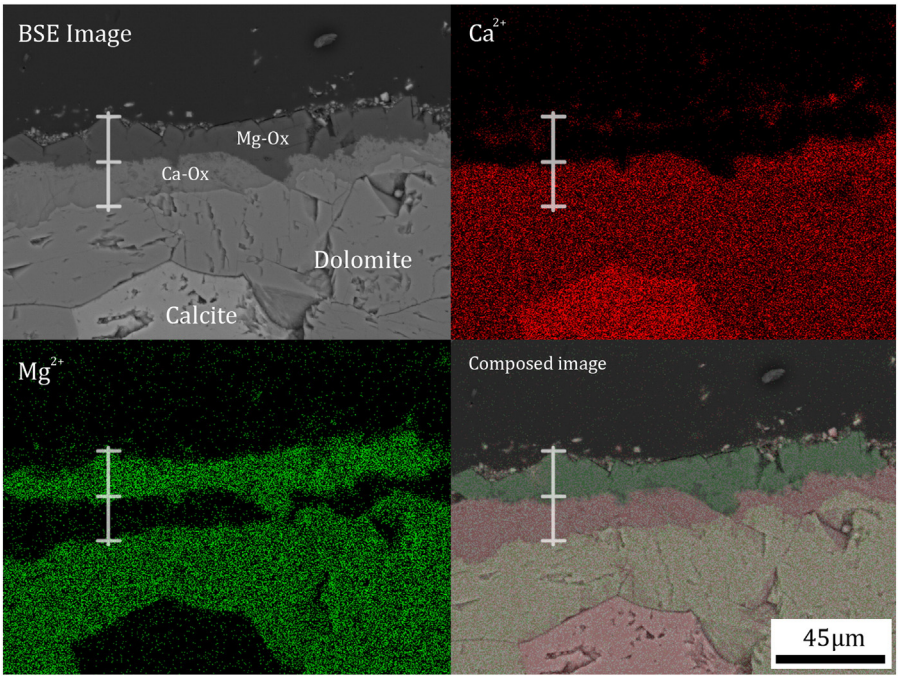

Fig. 4. BSE image and corresponding EDS map of a representative rim observed in a thin-section of D60 samples.

concentration increases as a result of dolomite dissolution until a point where a Mg oxalate phase can precipitate, as suggested by Kolo & Claeys [38]. However, the restricted spatial distribution of the Mg oxalate phase suggests that the high Mg concentrations necessary for its precipitation are only reached locally. In an attempt to confirm this possibility, the saturation index SI (SI = log(IAP/Ksp), where IAP is the ion activity product and Ksp the solubility product of a relevant phase of the solution with respect to the different relevant phases) and the solution speciation were modelled using the computer code Phreeqc ver. 3.1.7.9213 [39]. Marble-solution interaction is modelled assuming a continuous dissolution of dolomite coupled to oxalate mineral phases precipitation until equilibrium with respect to whewellite was reached. Simulations were done both at 25 °C and 60 °C, but negligible thermodynamic differences were found between both cases. Therefore, only the results from simulations done at 25 °C are presented in Fig. 5. In the case of the samples treated at 25 °C the calcium oxalate rim had an average thickness of ~10 μm (Fig. 3c) that corresponds to ~0.05 g of whewellite precipitated (Fig. 5, line a) over the whole marble block surface while in the case of the samples treated at 60 °C, the rim is ~30 μm thick (Fig. 3d), which corresponds to ~0.16 g of precipitated whewellite (Fig. 5, line b). As observed in Fig. 5, if we consider the above-mentioned amounts of precipitated whewellite, the SI for glushinskite would be higher than 0 (so that precipitation may occur) only in the case of samples treated at 60 °C. However, the low supersaturation values with respect to glushinskite found in Phreeqc simulations suggest very limited precipitation, consistent with the amount (<1%) of Mg oxalate phase observed in thin-sections of D60 samples. Such a low amount precluded the unambiguous identification of glushinskite (see Raman and XRD results, below).

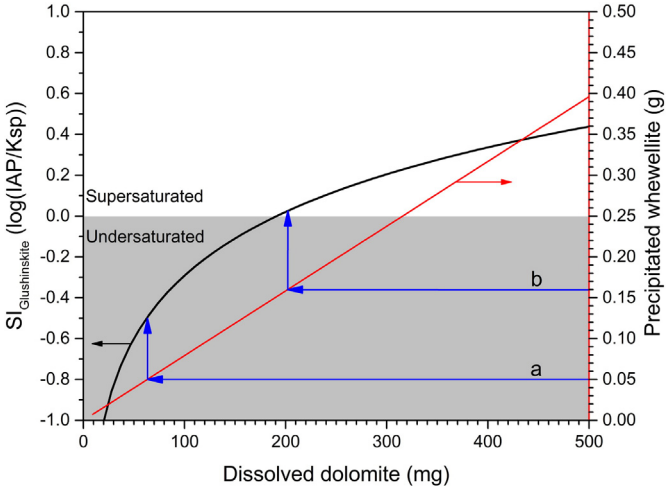

Fig. 5. Amount of precipitated whewellite and SI for glushinskite on dolomitic marble under the treatment conditions (25 °C, 100 mM Oxalic acid). Precipitated amount of whewellite corresponding to a) 10 μm thick rim and b) 30 μm thick rim. See text for details.

3.2. Mineralogical analysis

Micro-Raman analyses were performed directly on the marble surfaces (Fig. 6) Whewellite was identified on the surface of all treated

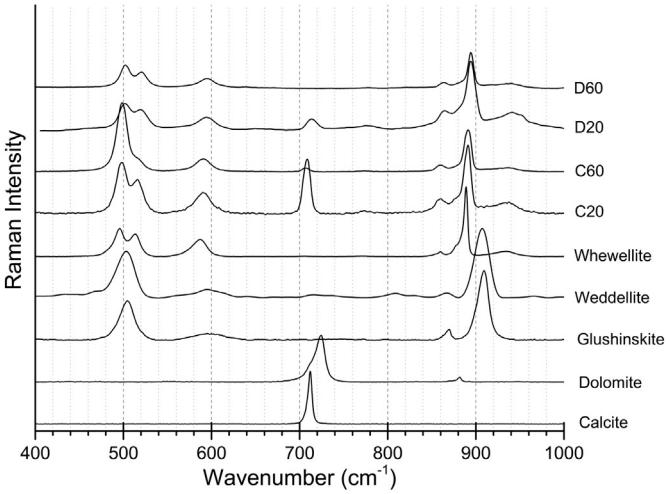

Fig. 6. Raman spectra of treated marble cubes. Reference spectra are from the RUFF database: calcite (R040070), dolomite (R040030), whewellite (R050526),weddellite (R050242) and glushinskite (R060318). RRUFF-ID in parenthesis.

marble samples by its characteristic bands at 939 (stretching υ_s(C—O)), 895 and 864 cm^{-1} (bending + δ(O—C═O)). Additionally, it was found that in samples C60 and D60 the bands at ca. 710 and 725 cm^{-1} (distinctive of $\upsilon_4(CO_3^{=})$ stretching for calcite and dolomite, respectively) were very weak or nearly undetectable due to the thicker oxalate rim compared to that of samples treated at a lower *T*. Weddellite ($CaC_2O_4 \cdot 2H_2O$) has been reported to be frequently present along with whewellite on carbonate stones [1,2,4,40]. However, both weddellite and glushinskite have almost the same Raman spectra with most of their bands overlapping or being too close to those of whewellite [41]. Therefore, an unambiguous identification of weddellite and/or glushinskite was not possible using this technique.

Fig. 6 also shows that in the case of treated dolomitic marble the main peak of whewellite at 895 cm^{-1} appeared shifted to higher wavenumbers. Such a shifting could be caused by the presence (in minor amounts) of glushinskite.

In order to identify which crystalline phases were present in the reaction rims, XRD analyses were performed (Fig. 7). For the probes treated at 60 °C, the corresponding Bragg peaks for calcite and dolomite in M60 and D60 samples respectively, were almost undetectable. Whewellite was the only identified oxalate mineral on the marble surfaces and the lack of peaks at 14.33 and 32.22 °2θ (which correspond to the most intense weddellite Bragg peaks) rules out the presence of weddellite. The absence of weddellite under the treatment conditions used here is not unexpected. In fact, Thongboonkerd et al. [42] found that only whewellite precipitated at pH < 5 under similar conditions than those used in this work. On the other hand, the non-clear presence of peaks at 18.11 (100%) and 28.14 (80%) °2θ, corresponding to the main Bragg peaks of glushinskite precludes an unambiguous identification of this crystalline phase on the treated dolomitic marble blocks. This is likely due to the relatively low amount of this phase in the reaction rim. However, we cannot rule out the possibility that the magnesium oxalate phase formed was amorphous to X-rays.

3.3. Treatment evaluation

At first, it might seem inappropriate to use an acid treatment for the conservation of (acid soluble) carbonate stones. However, the fact that the treatment application results in a fast neutralization of the acid and the rapid formation of an insoluble oxalate rim that limits the dissolution of the substrate to a few μm-thick surface layer, prevents additional acid-promoted dissolution (i.e., self-limiting effect). Note that all the existing conservation treatments based on the formation of an insoluble conversion layer, such as treatments using ammonium oxalate, di-ethyl oxalate, ammonium phosphate, and di-ammonium phosphate salts [22,26,27,29,43,44], involve the partial dissolution of the carbonate substrate. This results in the release of Ca ions that in turn precipitate as insoluble Ca oxalates or phosphates. In these cases, a thin surface layer of marble is also dissolved and transformed into the protective rim. However, because of the relatively high pH, these treatments occur via a non-coupled dissolution-precipitation processes (as explained in the introduction).

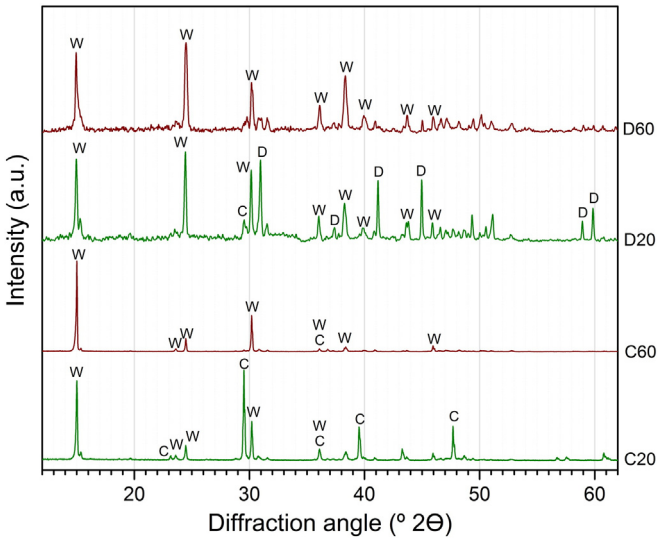

Fig. 7. X-Ray diffraction patterns of the surface of treated marble cubes. Legend: W, whewellite; D, dolomite; C, calcite.

After 7 days of treatment, no changes in sample size were detected using a micrometer caliper. Taking into account the block dimensions and molar volumes of whewellite, dolomite and calcite (65.87, 64.29 and 31.20 cm^3/mol, respectively), for the formation of a 30 μm thick whewellite rim, a 14.20 μm and a 29.2 μm thick layer of calcitic and dolomitic marble should have been dissolved, respectively. Note that because the pseudomorphic oxalate rim acts as a diffusion barrier, additional dissolution is kinetically limited. In fact, the formation of the oxalate rim is self-limited and never exceed a few tens of micrometers. Overall, these results show that the thickness of the dissolved marble surface and the newly formed oxalate rims is very similar. Furthermore, because the oxalate rim is pseudomorphic, it preserves the overall textural features of the pristine marble surface as shown in Fig. 3.

On the other hand, treated samples displayed thicker oxalate rims with increasing treatment temperature. This could be related to the higher amounts of Ca ions available for calcium oxalate rim growth because of *T*-enhanced marble substrate dissolution. The possibility that the high *T* treatment induced crack development in the marble substrate, thereby facilitating marble dissolution at increasing depths, cannot be ruled out (see MIP results, below).

Water absorption tests showed that the amount of water absorbed by the test cubes was very limited, due to the reduced porosity (<1.8%) [45] and small pore size of the Macael marble stones [46]. However, a slight increase in water absorption was observed after treatment (Fig. 8) as a consequence of porosity generation during treatment (see MIP results, below). In all cases, fast water absorption occurred during the first 4 min of the test, the untreated samples attaining absorption values similar to those reported previously [45,47]. Once a constant maximum free absorption value was reached, the forced water absorption capacity was determined (vacuum conditions). We observed that untreated calcitic and dolomitic marbles samples increase their weight by 0.13% and 0.23%, respectively, during water absorption test, in agreement with previous reports [47]. Finally, Fig. 8 shows that the desorption (i.e., drying) behavior was almost the same for treated and untreated samples in the case of the calcitic marble. In contrast, the drying rate decreased in the case of the treated dolomitic marble. Nevertheless, in all cases the amount of water retained can be considered as negligible. Thus, in this respect, the impact of the treatment would be minimal.

To evaluate possible treatment-related variations in porosity and pore size distribution, MIP analyses were performed. MIP analyses show that there was an increase in the total amount of pores after treatment (Fig. 9). It is likely that most of the porosity increase corresponds to the oxalate rims (analyzed samples corresponded to a 2 mm-thick slice of the marble surface), which were observed to be porous (OM and SEM results). However, a treatment-related (limited) porosity in the bulk marble cannot be ruled out. It is known that even moderate *T* values cause the opening of micro-cracks between calcite/dolomite grains in marble, increasing the porosity of the stone and, in most cases, increasing the number of large pores, thereby facilitating the penetration of water and solutions into intergranular spaces [22,47,48]. In the case of the calcitic marble, for both treatment temperatures, the cumulative pore volume increased from 2.1 mm^3/g (porosity, P = 0.57 ± 0.15%) up to 2.8 mm^3/g (P = 0.76 ± 0.30%) and for the dolomitic marble from 2.2 mm^3/g (P = 0.64 ± 0.14%) up to 3.8 mm^3/g (P = 1.11 ± 0.40%). These results are consistent with optical microscopy observations (Fig. 2) showing that the treated marble samples displayed more

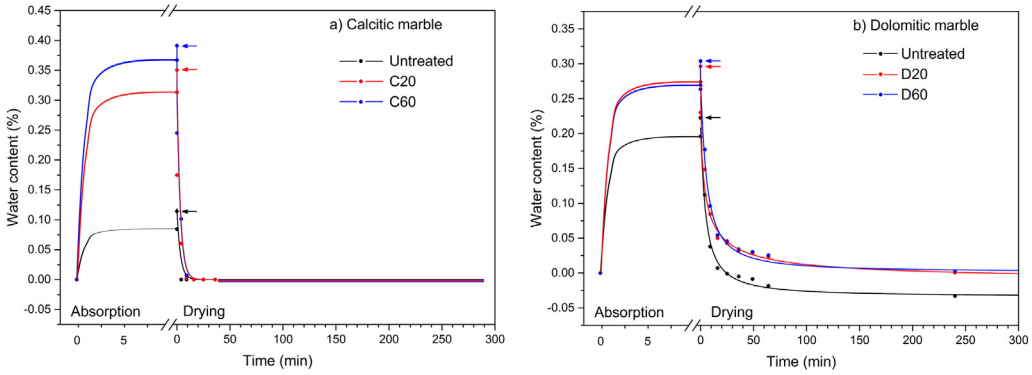

Fig. 8. Water absorption and drying of treated marble blocks. Variation of the amount of absorbed water (expressed as weight percentage) vs. time. a) Calcitic marble; b) Dolomitic marble. Errors bars have been omitted for the sake of clarity. The max SD (σ1) was 0.2 from 6 replicates.

abundant intra- and intergranular cracks than untreated marble samples. A substantial increase in the amount of pores with size between 5 and 30 μm, corresponding to cracks between grain boundaries [47], occurred after treatment application, especially in the case of the dolomitic marble (Fig. 9). Such effects may thus help to explain the observed increase in rim thickness found in samples treated at high *T*. They also help to explain why marble samples treated at 60 °C show higher water absorption values than untreated samples or samples treated at lower *T*. However, the absolutes values of porosity are quite low, which is consistent with the minor variations observed in the water absorption tests.

Water vapor permeability (WVP) tests (performed according to the EN 15803:2009) (Fig. 10) showed that in the case of the calcitic marble, the oxalate rim hindered water vapor permeability. Note that the higher the weight lost during the WVP tests, the greater the water vapor permeability of the sample. However, such a reduction was minimal. Interestingly, in the case of D20 samples, the permeability was also lower than that of the control (D) but it significantly increased in D60 samples. The latter effect seems to be related to porosity (cracks) generation inside the bulk marble. The developed oxalate rim acts as a permeability barrier hindering water vapor diffusion across the ~1 cm thick test probe as observed for the samples treated at 20 °C. However, considering thermal weathering of marbles [47,49] and the observed porosity generation (MIP results), it could be hypothesized that in the case of the dolomitic marble subjected to the higher *T* treatment, the hindering in water vapor permeability associated with the developed rim is overcome by a higher amount of intra- and intergranular cracks. Such cracks may facilitate water vapor diffusion through the bulk marble and, therefore, increase the overall water vapor permeability of D60 samples. In any case, the observed reduction or increase in water vapor permeability is minimal, as it is also minimal the water vapor permeability of these stones (due to their very low porosity).

The acid resistance tests showed that the developed oxalate rim protected marble stones in a very effective way against acid dissolution (initial pH of 4) due to the lower Ksp of whewellite (and Mg-oxalate, in the case of the dolomitic marble) compared to calcite and dolomite. It was found that the thicker the reaction rim formed on marble surface, the greater was the hindering of the Ca (and Mg) carbonate substrate dissolution. Increased thickness of the reaction rim would reduce the capacity of the dissolution products to diffuse through the rim. Here, it is clear that the protective rim acted as a diffusional barrier, reducing the dissolution rate of both the calcitic and dolomitic substrates, as inferred from the reduced rate of pH increase (Fig. 11a and b). SEM images were acquired both before and after 24 h acid attack of treated samples (Fig. 11c–f). In both the treated calcitic and dolimitic marble samples, no textural changes, such as crack development or calcium oxalate crystals dissolution, were observed after the acid attack. These observations are consistent with those of Doherty et al. [11] showing no changes in the oxalate conversion layer formed on calcitic marble surfaces treated with an ammonium-oxalate solution, following acid attack. Moreover, our SEM images show an epitaxial relationship between whewellite crystals and calcite crystals in the calcitic marble, as demonstrated by the clear preferred orientation of oxalate crystals (Fig. 11c and Figs. S3 and S4) [30]. Such a preferred crystallographic orientation was not observed in the case of the dolomitic marble, where randomly oriented whewellite crystals were systematically observed (Fig. 11d and f, and Fig. S5). These results can be related to the higher structural matching that exists between whewellite and calcite (favoring an epitaxial nucleation and growth of whewellite crystals) [30], as compared with that of whewellite and dolomite. This explains why in the case of the treated

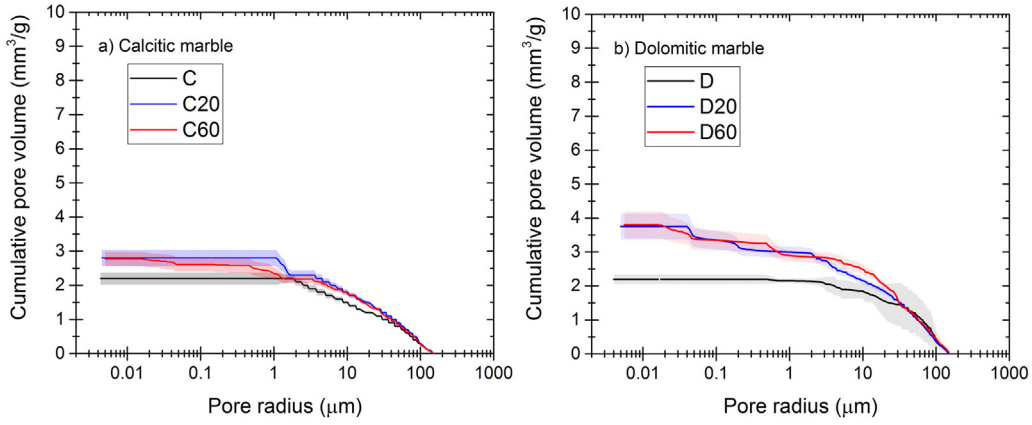

Fig. 9. Mercury intrusion porosimetry (MIP) analysis of treated samples and untreated samples for the (a) calcitic and (b) dolomitic marbles. Lines show average from 2 replicates and the shaded area show $2\sigma_N$.

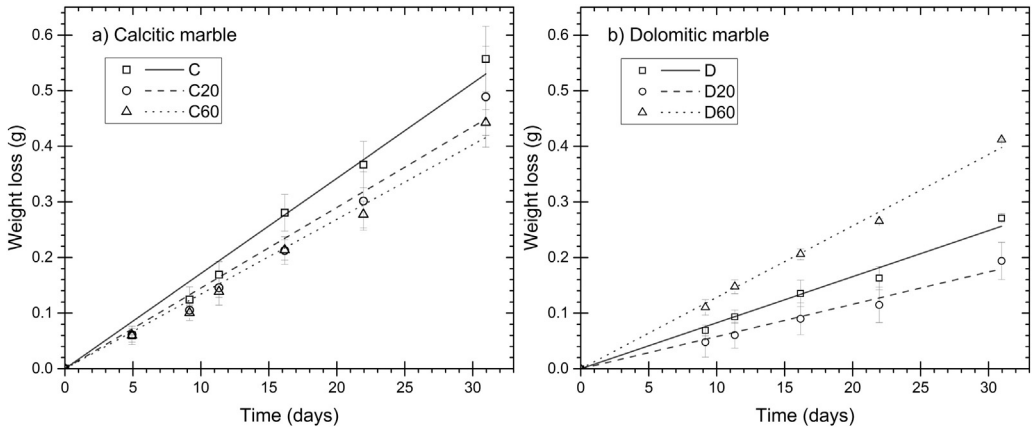

Fig. 10. Time-dependent weight loss during water vapor permeability tests. a) Calcitic marble; b) Dolomitic marble. Errors bar show $2\sigma_N$ from 5 replicates.

dolomitic marble samples, smaller crystal sizes and a less compact and more porous structure, were observed (Fig. 11d and f, and Fig. S5), as compared with the treated calcitic marble (Fig. 11c and e, and Figs. S3 and S4). The formation of such a less compact and more porous oxalate film explains why after 24 h acid attack the dolomitic marble samples treated at 20 °C (D20), which developed a whewellite film ~10 μm in thickness, reached a final pH value of ~7.5. In the case of the dolomitic marble samples treated at 60 °C, it should be considered that despite the smaller oxalate crystal sizes, and the less compact and more porous structure observed by means of SEM (Fig. 11f), the thicker oxalate film (~30 μm in thickness) offered a more effective diffusional barrier, thereby resulting in a higher protection against acid attack as demonstrated by the limited pH increase during acid testing.

These results may seem counterintuitive when one considers that marble samples with thicker oxalate rims (high *T* treatment) display a slightly higher porosity and water absorption. The latter should mean that the rim is more permeable. However, as indicated above, the increase in porosity and water absorption capacity is minimal and, apparently, not enough to enable/favor the access of the acid solution to the marble substrate.

The results of the SO_2 ageing test showed that the treatment was successful at protecting marble again chemical weathering. The typical effect of SO_2 on calcitic substrates is the replacement of calcium carbonate by gypsum ($CaSO_4 \cdot 2H_2O$), generating massive efflorescence that typically cover the surface, thereby having a significant aesthetic impact. Similarly, in the case of a dolomitic substrate, SO_2 attack typically results in the formation of gypsum and epsomite ($MgSO_4 \cdot 7H_2O$) efflorescence [50]. Therefore, a protective treatment against this deleterious phenomenon is essential for cultural heritage preservation. It was found that the generated oxalate rims protected marble stones against SO_2 in a very effective way. Such a protective effect was higher the thicker the rim was. Fig. 12 shows FESEM photomicrographs of marble surfaces after 21 days SO_2 exposure. It can be seen that when the oxalate rim was thicker (i.e. C60 and D60 samples), the amount and surface coverage of newly formed gypsum crystals decreased.

An evaluation of possible color changes associated with the application of a conservation treatment is critical to decide whether such a treatment can be used in practical applications without affecting the appearance of the stone surface. Fig. 13a shows that average values of ΔE_{00} (color change) for most of treated and untreated marble samples were

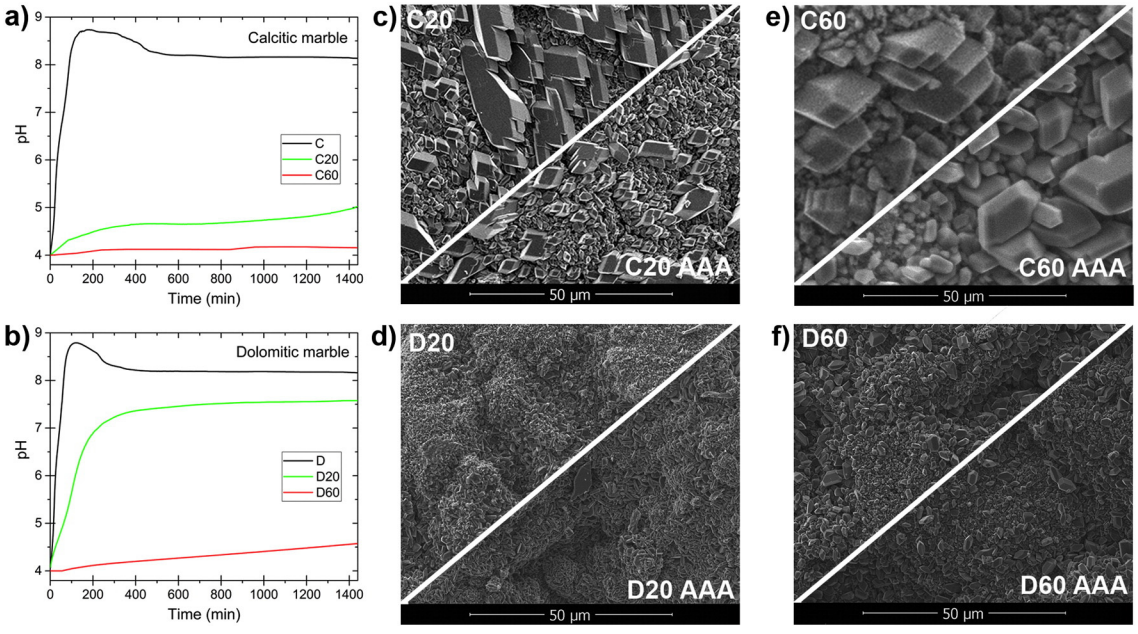

Fig. 11. Acid resistance tests. Time-evolution of solution pH for the treated and untreated calcitic (a) and dolomitic (b) marble probes starting with a 150 mL hydrochloric acid with an initial pH of 4. SEM images of calcitic (c) and dolomitic (d) marble probes treated at 20 °C before and After 24 h of Acid Attack (AAA). SEM images of calcitic (e) and dolomitic (f) marble probes treated at 60 °C before and after 24 h of acid attack.

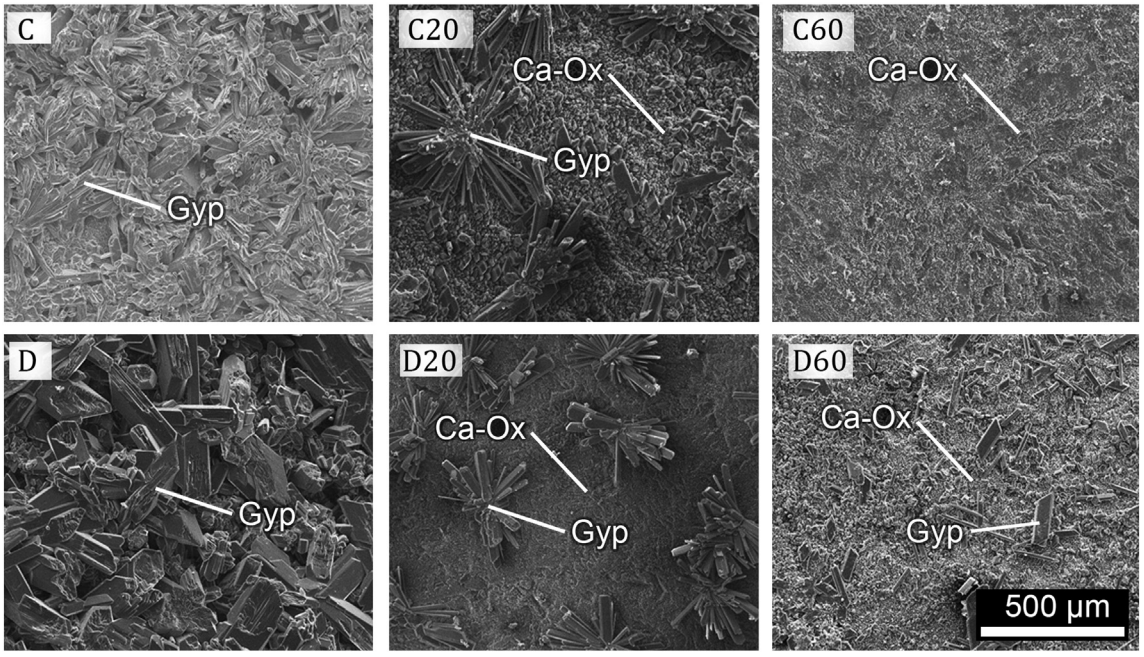

Fig. 12. FESEM photomicrographs of SO_2 aged treated and untreated marble samples. Legend: Gyp: Gypsum, Ca-Ox: Calcium oxalate.

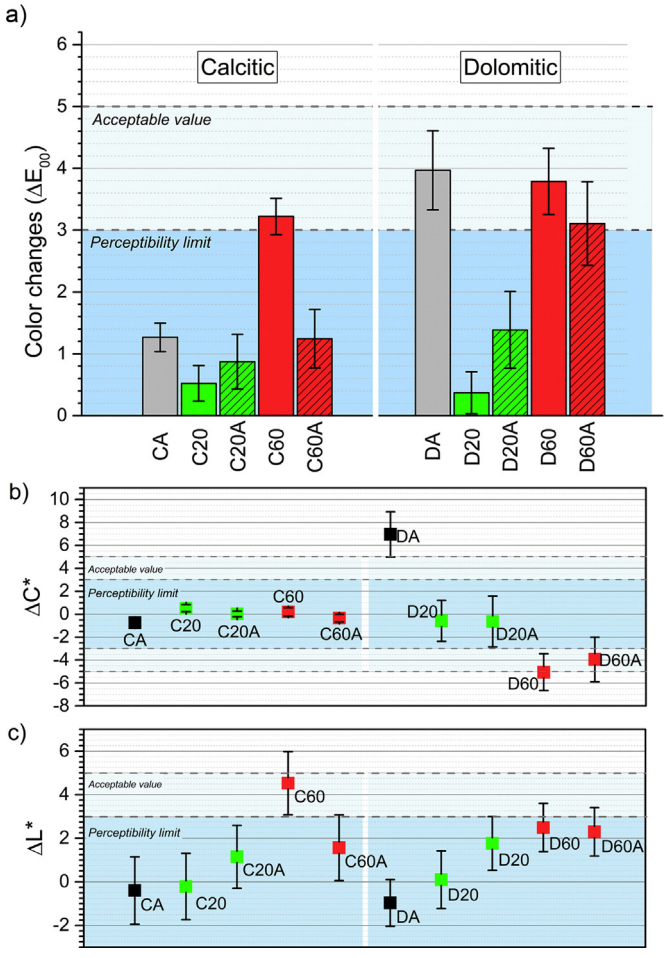

Fig. 13. a) Color changes according to ΔE_{00} (CIEDE2000) and variations in b) chroma (ΔC^*) and c) luminosity (ΔL^*). Error bars show $2\sigma_N$ ($N \geq 18$).

just at or below the perceptibility limit for the human eye ($\Delta E_{00} = 3$) [51].

Only the samples treated at 60 °C had a ΔE_{00} value slightly higher than 3, but still below 5, the threshold value considered as acceptable for an adequate consolidation or protective treatment [51–53]. However, the validity of ΔE_{00} is currently questioned [33,51,52], because the human eye is more sensitive to certain colors than others, which means that certain ΔE_{00} could be insignificant for the eye despite having a high value. Hence, differences in the chroma (ΔC^*) and lightness (ΔL^*) components (Fig. 13b and c) were also analyzed. Despite the massive gypsum growth observed in FESEM images (Fig. 12) of untreated aged samples, color measurements shown a low ΔE_{00} value due to the similarities in color and brightness between the newly formed gypsum crust and the initial marble surface. However, a whitening effect was detected for both untreated and treated samples after the SO_2 test. In other words, the color intensity, C^* tended to decrease ($\Delta C^* < 0$), while L^* increased ($\Delta L^* > 0$). In the case of the calcitic marble, the main color differences were due to changes in lightness while in the case of the dolomitic marble were also due to changes in chroma (Fig. 13b). In the case of the dolomitic marble the higher color differences were found in samples treated at 60 °C. Only in the case of the untreated dolomitic marble samples that were aged (DA) a value above the acceptable limits in the chroma component was found. All samples treated at 20 °C presented lower color differences than both samples treated at 60 °C and untreated ones.

4. Conclusions

The application of oxalic acid solutions on the two selected types of marble resulted in the development of a very coherent rim (conversion layer) made of whewellite (and Mg-oxalate, in the case of the tested dolomitic marble). The textural and microstructural features of these conversion layers are consistent with their formation via an interface coupled dissolution-precipitation process in which the oxalate superficial layer reproduced the initial topography of the substrate, thereby resulting in a pseudomorphic replacement.

The tests carried out to assess the efficacy of the treatment show that, in general,

(i) The higher the treatment *T* the greater the developed rim thickness. However, moderately high treatment *T* (i.e., 60 °C) could

be counterproductive due to thermal weathering and possible associated crack development.

(ii) The oxalate rim protects against chemical weathering (dissolution) providing the treated marble stones with a higher acid resistance.

(iii) The water-marble interactions were modified in terms of a slight increase in water absorption (mainly due to the porosity generated by the rim development) and a decrease (~20%) in water vapor permeability except for the dolomitic marble samples treated at 60 °C in which the water vapor permeability increases (~40%), likely due to thermal-induced crack development. However, all values were extremely low.

(iv) Color changes were almost negligible in all the samples except for the untreated samples that were aged (SO_2 attack) in which a large amount of gypsum efflorescence developed, thereby showing a whitening effect.

In summary, our results show that this treatment is viable and highly effective for the protection of this type of stone materials, especially in elements such as statues and other marble elements not subjected to continuous friction forces (as it could be the case of floors) but exposed to environments where chemical weathering (e.g. dissolution or salt crystallization due to acid rain and/or environmental pollution related to gases such as SO_2 or NO_x) may occur. On the other hand, the higher the treatment *T*, the greater its efficiency in terms of resistance against chemical attack because of a greater rim thickness. However, high treatment *T* could induce thermal weathering. Therefore, it is recommended that treatment application is carried out with a soft local heating of the area or heating the oxalic acid solution prior to application but avoiding the heating of the whole piece to be treated. The application method of such a treatment could be a short-time immersion in an acid solution if possible (e.g. small sculptures), application of oxalic acid-loaded poultices or brushing/spraying of the solution on larger parts such as surfaces of building elements.

Supplementary data to this article can be found online at http://dx.doi.org/10.1016/j.matdes.2016.11.037.

Acknowledgements

This work was financially supported by the Spanish Government (Grants MAT2012-37584, CGL2012-35992 and CGL2015-70642-R) and the Junta de Andalucía (Research Group RNM-179 and Project P11-RNM-7550). E.R.-A. acknowledges a Ramón y Cajal grant. We thank the Centro de Instrumentación Científica (CIC; University of Granada) for analytical assistance.

References

[1] P. Maravelaki-Kalaitzaki, Black crusts and patinas on Pentelic marble from the Parthenon and Erechtheum (Acropolis, Athens): characterization and origin, Anal. Chim. Acta 532 (2005) 187–198, http://dx.doi.org/10.1016/j.aca.2004.10.065.

[2] J. Hällström, K. Barup, R. Grönlund, A. Johansson, S. Svanberg, L. Palombi, et al., Documentation of soiled and biodeteriorated facades: a case study on the Coliseum, Rome, using hyperspectral imaging fluorescence lidars, J. Cult. Herit. 10 (2009) 106–115, http://dx.doi.org/10.1016/j.culher.2008.04.008.

[3] M. Del Monte, C. Sabbioni, G. Zappia, The origin of calcium oxalates on historical buildings, monuments and natural outcrops, Sci. Total Environ. 67 (1987) 17–39, http://dx.doi.org/10.1016/0048-9697(87)90063-5.

[4] G. Hyvert, Les Statues de Rapa Nui, conservation et restauration: Île de Pâques - (mission) février-mars 1972, UNESCO Doc. 2868/RMO.R, 47, 1973.

[5] L. Rampazzi, Analytical investigation of calcium oxalate films on marble monuments, Talanta 63 (2004) 967–977, http://dx.doi.org/10.1016/j.talanta.2004.01.005.

[6] G.M. Gadd, J. Bahri-Esfahani, Q. Li, Y.J. Rhee, Z. Wei, M. Fomina, et al., Oxalate production by fungi: significance in geomycology, biodeterioration and bioremediation, Fungal Biol. Rev. 28 (2014) 36–55, http://dx.doi.org/10.1016/j.fbr.2014.05.001.

[7] L. Lazzarini, O. Salvadori, A reassessment of the formation of the patina called scialbatura, Stud. Conserv. 34 (1989) 20–26, http://dx.doi.org/10.1179/sic.1989.34.1.20.

[8] J.L. Perez-Rodriguez, A. Duran, M.A. Centeno, J.M. Martinez-Blanes, M.D. Robador, Thermal analysis of monument patina containing hydrated calcium oxalates, Thermochim. Acta 512 (2011) 5–12, http://dx.doi.org/10.1016/j.tca.2010.08.015.

[9] J. Stannard, Medicinal plants and folk remedies in Pliny, "Historia Naturalis,", Hist. Philos. Life Sci. 4 (1982) 3–23.

[10] F. Davidovits, J. Aliaga, Fabrication of Stone objects, by geopolymeric synthesis, in the pré-incan Huanka civilisation (Peru), XXI Archeometry Symp., 1981 (Brookhaven, UK.).

[11] B. Doherty, M. Pamplona, R. Selvaggi, C. Miliani, M. Matteini, A. Sgamellotti, et al., Efficiency and resistance of the artificial oxalate protection treatment on marble against chemical weathering, Appl. Surf. Sci. 253 (2007) 4477–4484, http://dx.doi.org/10.1016/j.apsusc.2006.09.056.

[12] O. Salvadori, A.C. Municchia, The role of fungi and lichens in the biodeterioration of stone monuments, Open Conf. Proc. J. 7 (2016) 39–54, http://dx.doi.org/10.2174/2210289201607020039.

[13] M. Lisci, M. Monte, E. Pacini, Lichens and higher plants on stone: a review, Int. Biodeterior. Biodegrad. 51 (2003) 1–17, http://dx.doi.org/10.1016/S0964-8305(02)00071-9.

[14] M. Monte, Oxalate film formation on marble specimens caused by fungus, J. Cult. Herit. 4 (2003) 255–258, http://dx.doi.org/10.1016/S1296-2074(03)00051-7.

[15] A.V. Rusakov, A.D. Vlasov, M.S. Zelenskaya, O.V. Frank-Kamenetskaya, D.Y. Vlasov, The Crystallization of Calcium Oxalate Hydrates Formed by Interaction Between Microorganisms and Minerals, 2016 357–377, http://dx.doi.org/10.1007/978-3-319-24987-2_28.

[16] R.I. Dorn, L. Vinet, A. Zhedanov, in: A.J. Parsons, A.D. Abrahams (Eds.), Desert Rock Coatings BT - Geomorphology of Desert Environments, J. Phys. A Math. Theor., Springer Netherlands, Dordrecht 2009, pp. 153–186, http://dx.doi.org/10.1007/978-1-4020-5719-9_7.

[17] J. Chen, H.P. Blume, L. Beyer, Weathering of rocks induced by lichen colonization - a review, Catena 39 (2000) 121–146, http://dx.doi.org/10.1016/S0341-8162(99)00085-5.

[18] M. Monte, Lichens on Monuments: Enviromental Bioindicators, Sci. Technol. Eur. Cult. Herit., Elsevier, 1991 355–359, http://dx.doi.org/10.1016/B978-0-7506-0237-2.50044-7.

[19] E.V. Sturm (née Rosseeva), O. Frank-Kamenetskaya, D. Vlasov, M. Zelenskaya, K. Sazanova, A. Rusakov, et al., Crystallization of calcium oxalate hydrates by interaction of calcite marble with fungus Aspergillus niger, Am. Mineral. 100 (2015) 2559–2565, http://dx.doi.org/10.2138/am-2015-5104.

[20] C.M. Belfiore, G.V. Fichera, M. Francesco, L. Russa, A. Pezzino, S.A. Ruffolo, et al., The Baroque Architecture of Scicli (South-eastern Sicily): Characterization of Degradation Materials and Testing of Protective Products, 2012 19–33, http://dx.doi.org/10.2451/2012PM0002.

[21] C. Saiz-Jimenez, Biogenic vs anthropogenic oxalic acid in the environment, Oxalate Film. Orig. Mean. Conserv. Work. Art, Centro del C.N.R. "Gino Bozza," Milan, 1989.

[22] E. Sassoni, G. Graziani, E. Franzoni, Repair of sugaring marble by ammonium phosphate: comparison with ethyl silicate and ammonium oxalate and pilot application to historic artifact, Mater. Des. 88 (2015) 1145–1157, http://dx.doi.org/10.1016/j.matdes.2015.09.101.

[23] H.E. King, D.C. Mattner, O. Plümper, T. Geisler, A. Putnis, Forming cohesive calcium oxalate layers on marble surfaces for stone conservation, Cryst. Growth Des. 14 (2014) 3910–3917, http://dx.doi.org/10.1021/cg500495a.

[24] E. Doehne, C.A. Price, Stone Conservation: An Overview of Current Research, Getty Conservation Institute, Los Angeles, California, 2011.

[25] T.M. Cezar, Calcium oxalate: a surface treatment for limestone, Archit. Stone Carving Course 4 (1998) 6, http://dx.doi.org/10.5334/jcms.4982.

[26] D. Mudronja, F. Vanmeert, K. Hellemans, S. Fazinic, K. Janssens, D. Tibljas, et al., Efficiency of applying ammonium oxalate for protection of monumental limestone by poultice, immersion and brushing methods, Appl. Phys. A Mater. Sci. Process. 111 (2013) 109–119, http://dx.doi.org/10.1007/s00339-012-7365-9.

[27] C. Conti, C. Colombo, D. Dellasega, M. Matteini, M. Realini, G. Zerbi, Ammonium oxalate treatment: evaluation by μ-Raman mapping of the penetration depth in different plasters, J. Cult. Herit. 12 (2011) 372–379, http://dx.doi.org/10.1016/j.culher.2011.03.004.

[28] C. Conti, I. Aliatis, M. Casati, C. Colombo, M. Matteini, R. Negrotti, et al., Diethyl oxalate as a new potential conservation product for decayed carbonatic substrates, J. Cult. Herit. 15 (2014) 336–338, http://dx.doi.org/10.1016/j.culher.2013.08.002.

[29] L. Maiore, M.C. Aragoni, G. Carcangiu, O. Cocco, F. Isaia, V. Lippolis, et al., Synthesis, characterization and DFT-modeling of novel agents for the protection and restoration of historical calcareous stone substrates, J. Colloid Interface Sci. 448 (2015) 320–330, http://dx.doi.org/10.1016/j.jcis.2015.01.092.

[30] E. Ruiz-Agudo, P. Álvarez-Lloret, C.V. Putnis, a.B. Rodriguez-Navarro, A. Putnis, Influence of chemical and structural factors on the calcite–calcium oxalate transformation, CrystEngComm 15 (2013) 9968, http://dx.doi.org/10.1039/c3ce41294f.

[31] AENOR, Natural Stone Test Methods. Determination of Water Absorption at Atmospheric Pressure(UNE-EN 13755:2008, Madrid) 2008.

[32] AENOR, Conservation of Cultural Property. Test Methods. Determination of Water Vapour Permeability(UNE-EN 15803:2010, Madrid) 2010.

[33] G. Sharma, W. Wu, E.N. Dalal, The CIEDE2000 color-difference formula: implementation notes, supplementary test data, and mathematical observations, Color. Res. Appl. 30 (2005) 21–30, http://dx.doi.org/10.1002/col.20070.

[34] AENOR, Natural Stone Test Methods. Determination of Resistance to Ageing by SO2 Action in the Presence of Humidity(UNE-EN 13919:2003, Madrid) 2003.

[35] L. Brečević, D. Škrtić, J. Garside, Transformation of calcium oxalate hydrates, J. Cryst. Growth 74 (1986) 399–408, http://dx.doi.org/10.1016/0022-0248(86)90131-4.

[36] W.M. Haynes, CRC Handbook of Chemistry and Physics, 96th ed. CRC Press, 2015.
[37] A. Putnis, Mineral replacement reactions, Rev. Mineral. Geochem. 70 (2009) 87–124, http://dx.doi.org/10.2138/rmg.2009.70.3.
[38] K. Kolo, P. Claeys, In vitro formation of Ca-oxalates and the mineral glushinskite by fungal interaction with carbonate substrates and seawater, Biogeosci. Discuss. 2 (2005) 451–497, http://dx.doi.org/10.5194/bgd-2-451-2005.
[39] D.L. Parkhurst, C.A.J. Appelo, Description of input and examples for PHREEQC version 3–a computer program for speciation, batch-reaction, one-dimensional transport, and inverse geochemical calculations, U.S. Geol. Surv. Tech. Methods, B. 6 (2013) 497 (Chapter A43).
[40] C. Conti, I. Aliatis, C. Colombo, M. Greco, E. Possenti, M. Realini, et al., u-Raman mapping to study calcium oxalate historical films, J. Raman Spectrosc. 43 (2012) 1604–1611, http://dx.doi.org/10.1002/jrs.4072.
[41] R.L. Frost, K.L. Erickson, M.L. Weier, P. Leverett, P.a. Williams, Raman spectroscopy of likasite at 298 and 77 K, Spectrochim. Acta A Mol. Biomol. Spectrosc. 61 (2005) 607–612, http://dx.doi.org/10.1016/j.saa.2004.05.014.
[42] V. Thongboonkerd, T. Semangoen, S. Chutipongtanate, Factors determining types and morphologies of calcium oxalate crystals: molar concentrations, buffering, pH, stirring and temperature, Clin. Chim. Acta 367 (2006) 120–131, http://dx.doi.org/10.1016/j.cca.2005.11.033.
[43] P. Meloni, F. Manca, G. Carcangiu, Marble protection: an inorganic electrokinetic approach, Appl. Surf. Sci. 273 (2013) 377–385, http://dx.doi.org/10.1016/j.apsusc.2013.02.048.
[44] G. Graziani, E. Sassoni, E. Franzoni, G.W. Scherer, Hydroxyapatite coatings for marble protection: optimization of calcite covering and acid resistance, Appl. Surf. Sci. 368 (2016) 241–257, http://dx.doi.org/10.1016/j.apsusc.2016.01.202.
[45] A. Luque, G. Cultrone, S. Mosch, S. Siegesmund, E. Sebastian, B. Leiss, Anisotropic behaviour of white Macael marble used in the Alhambra of Granada (Spain), Eng. Geol. 115 (2010) 209–216, http://dx.doi.org/10.1016/j.enggeo.2009.06.015.
[46] M.P. Sáez-Pérez, J. Rodríguez-Gordillo, Structural and compositional anisotropy in Macael marble (Spain) by ultrasonic, XRD and optical microscopy methods, Constr. Build. Mater. 23 (2009) 2121–2126, http://dx.doi.org/10.1016/j.conbuildmat.2008.10.013.
[47] A. Luque, E. Ruiz-Agudo, G. Cultrone, E. Sebastián, S. Siegesmund, Direct observation of microcrack development in marble caused by thermal weathering, Environ. Earth Sci. 62 (2011) 1375–1386, http://dx.doi.org/10.1007/s12665-010-0624-1.
[48] E. Sassoni, E. Franzoni, Influence of porosity on artificial deterioration of marble and limestone by heating, Appl. Phys. A Mater. Sci. Process. 115 (2014) 809–816, http://dx.doi.org/10.1007/s00339-013-7863-4.
[49] E. Franzoni, E. Sassoni, G.W. Scherer, S. Naidu, Artificial weathering of stone by heating, J. Cult. Herit. 14 (2013) e85–e93, http://dx.doi.org/10.1016/j.culher.2012.11.026.
[50] G. Cultrone, A. Arizzi, E. Sebastián, C. Rodriguez-Navarro, Sulfation of calcitic and dolomitic lime mortars in the presence of diesel particulate matter, Environ. Geol. 56 (2008) 741–752, http://dx.doi.org/10.1007/s00254-008-1379-9.
[51] D. Benavente, F. Martínez-Verdú, A. Bernabeu, V. Viqueira, R. Fort, M.A. García del Cura, et al., Influence of surface roughness on color changes in building stones, Color. Res. Appl. 28 (2003) 343–351, http://dx.doi.org/10.1002/col.10178.
[52] N.S. Baer, R. Snethlage, Saving our Architectural Heritage: The Conservation of Historic Stone Structures, Wiley, 1997.
[53] C.M. Belfiore, M.F. Russa, A. Pezzino, E. Campani, A. Casoli, The Baroque monuments of Modica (Eastern Sicily): assessment of causes of chromatic alteration of stone building materials, Appl. Phys. A Mater. Sci. Process. 100 (2010) 835–844, http://dx.doi.org/10.1007/s00339-010-5659-3.